International Journal of Thermal Sciences 49 (2010) 1103–1114

Contents lists available at ScienceDirect

International Journal of Thermal Sciences

journal homepage: www.elsevier.com/locate/ijts

Visualisation of heat transfer in 3D unsteady flows

M.F.M. Speetjens*, A.A. van Steenhoven

Department of Mechanical Engineering, Eindhoven University of Technology, P.O. Box 513 5600 MB, Eindhoven, The Netherlands

ARTICLE INFO

Article history:
Received 30 June 2009
Received in revised form
7 January 2010
Accepted 10 January 2010
Available online 11 February 2010

Keywords:
Heat-transfer visualisation
Laminar flow
Lagrangian analysis
Chaotic heat transfer
Numerical simulation

ABSTRACT

Heat transfer in fluid flows traditionally is examined in terms of temperature field and heat-transfer coefficients at non-adiabatic walls. However, heat transfer may alternatively be considered as the transport of thermal energy by the total convective–conductive heat flux in a way analogous to the transport of fluid by the flow field. The paths followed by the total heat flux are the thermal counterpart to fluid trajectories and facilitate heat-transfer visualisation in a similar manner as flow visualisation. This has great potential for applications in which insight into the heat fluxes throughout the entire configuration is essential (e.g. cooling systems, heat exchangers). To date this concept has been restricted to 2D steady flows. The present study proposes its generalisation to 3D unsteady flows by representing heat transfer as the 3D unsteady motion of a virtual fluid subject to continuity. This unified ansatz enables heat-transfer visualisation with well-known geometrical methods from laminar-mixing studies. These methods lean on the property that continuity "organises" fluid trajectories into sets of coherent structures ("flow topology") that geometrically determine the fluid transport. Decomposition of the flow topology into its constituent coherent structures visualises the transport routes and affords insight into the transport properties. Thermal trajectories form a thermal topology of essentially equivalent composition that can be visualised by the same methodology. This thermal topology is defined in both flow and solid regions and thus describes the heat transfer throughout the entire domain of interest. The heat-transfer visualisation is provided with a physical framework and demonstrated by way of representative examples.

1. Introduction

Industrial heat transfer problems may roughly be classified into two kinds of configurations. First, configurations in which the goal is rapid achievement of a uniform temperature field from a non-uniform initial state ("thermal homogenisation"). Second, configurations in which the goal is accomplishment and maintenance of high heat-transfer rates in certain directions. Thermal homogenisation is relevant for attainment of uniform product properties and processing conditions (e.g. during fabrication of polymers, glass, steel) and its key determinant is the temporal evolution of the temperature field towards its desired uniform state [1,2]. This evolution is dictated by so-called dominant eigenmodes of the advection-diffusion[1] operator; these eigenmodes cause the temperature field to rapidly assume a given spatial distribution that decays exponentially towards a homogeneous state [2–4]. Sustained high heat-transfer rates are relevant for heat exchangers, cooling applications and certain stages of the thermal processing of materials (e.g. tempering of polymer melts) and the key determinants here are the direction and intensity of heat fluxes [5–7]. The present study concentrates on the latter kind of heat-transfer problems and then specifically under laminar flow conditions. This is motivated by the persistent relevance of viscous thermofluids (polymers, glass, steel) and, in particular, by the growing importance of compact applications due to process intensification and continuous miniaturisation of heat-transfer and thermal-processing equipment [8–11], the rapid development of micro-fluidics [12–16] and the rising thermal challenges in electronics cooling [17–22].

Heat transfer traditionally is examined in terms of convective heat-transfer coefficients at non-adiabatic walls as a function of the flow conditions [2,5,6,8,23–27]. However, heat transfer may alternatively be considered as the transport of thermal energy by the *total* convective–conductive heat flux in a way analogous to the transport of fluid by the flow field. The paths followed by the total heat flux are the thermal counterpart to fluid trajectories and facilitate heat-transfer visualisation in a similar manner as flow

* Corresponding author. Tel.: +31 40 247 5428; fax: +31 40 243 3445.
E-mail addresses: m.f.m.speetjens@tue.nl (M.F.M. Speetjens), a.a.v.steenhoven@tue.nl (A.A. van Steenhoven).

[1] Some terminology: advection is transport by fluid motion; diffusion is transport by molecular motion. In heat-transfer problems, advection and diffusion are usually denoted "convection" and "conduction," respectively. Here both nomenclatures are used interchangeably.

1290-0729/$ – see front matter © 2010 Elsevier Masson SAS. All rights reserved.
doi:10.1016/j.ijthermalsci.2010.01.012

Nomenclature

c_h	specific heat (J/kg K)
e	internal energy (J/kg)
$\boldsymbol{M}$	(non-dimensional) mass flux (kg/m^2 s)
L	characteristic length scale (m)
p	pressure (Pa)
$Pe = \frac{\rho_0 c_h UL}{\lambda} = \frac{UL}{\alpha}$	Péclet number
$\boldsymbol{q}$	(non-dimensional) conductive heat flux (W/m^2)
q_H	volumetric heat source (W/m^3)
$\boldsymbol{q}_c$	convective heat flux (W/m^2)
$\boldsymbol{Q}$	(non-dimensional) total heat flux (W/m^2)
$Re = \frac{UL}{\nu}$	Reynolds number
t	(non-dimensional) time (s)
T	(non-dimensional) temperature (K)
T_{min}	minimum temperature (K)
T_{max}	maximum temperature (K)
$\boldsymbol{u}$	(non-dimensional) fluid velocity (m/s)
U	characteristic velocity (m/s)
x	(non-dimensional) horizontal coordinate (m)
y	(non-dimensional) vertical coordinate (m)
$\boldsymbol{x}$	(non-dimensional) fluid trajectory (m)
$\boldsymbol{x}_T$	(non-dimensional) thermal trajectory (m)

Greek symbols

α	thermal diffusivity (m^2/s)
β	thermal expansivity (1/K)
ϵ	amplitude of time-periodic fluctuations
λ	thermal conductivity (W/m K)
Λ	ratio of thermal conductivities at fluid–solid interface
Π	non-dimensional thermal expansivity
Ψ	(non-dimensional) stream function (kg/m s)
Ψ_T	(non-dimensional) thermal stream function (W/m)
ρ	fluid density (kg/m^3)
$\boldsymbol{\sigma}$	viscous stress tensor (Pa)
τ	(non-dimensional) period time (s)

Subscripts

0	characteristic quantity
o	quantity related to solid object
T	thermal quantity
x	horizontal vector component
y	vertical vector component

visualisation. This concept has originally been introduced by [28] for 2D steady flows and has found application in a wide range of studies. Examples include investigations on convective heat transfer in general [7,29], total energy flows (comprising thermal, potential, kinetic, magnetic, electrical and chemical contributions) [30], heat transfer in reacting flows [31], electronics cooling [32] and natural convection in the presence of porous walls [33,34]. In 2D steady systems the thermal trajectories are defined by a thermal stream function; a generalisation to 3D steady flows is proposed in [30] by identifying the 3D thermal trajectories with the field lines of the 3D heat-flux vector. Heat-transfer visualisation in unsteady flows is hitherto restricted to steady-state approximations to time-averaged 2D time-periodic flows [30] and weakly-unsteady flows [35]. However, ways for truly 3D unsteady heat-transfer visualisation are lacking to date. The present study seeks to bridge this gap by proposing a method for heat-transfer visualisation in generic 3D unsteady flows. This hinges on the unified Lagrangian transport formalism for generic scalar transport in laminar flows by [36].

Key to the unified Lagrangian approach is the fundamental property that fluid and thermal trajectories both are subject to an equivalent continuity constraint and thus, inherently, to the same geometrical restrictions. Hence, in the trajectory-based (i.e. *Lagrangian*) representation, fluid and heat transfer admit a unified description as the motion of a (virtual) fluid subject to continuity [36]. This ansatz is particularly suited for laminar flows, where fluid and thermal trajectories are well-defined, and thus has great potential for the thermal analysis of the (compact) heat-transfer problems that motivate this study. The Lagrangian approach e.g. enables, similar to its proven strength in studies on chaotic advection, direct investigation of the mechanisms underlying chaotic heat transfer and its role in the heat-transfer properties of a given configuration.

The analogy with (laminar) fluid motion enables heat-transfer visualisation by well-established geometrical methods from laminar-mixing studies [12,14,37–40]. These methods lean on the property that continuity "organises" fluid trajectories into sets of coherent structures ("flow topology) that geometrically determine the fluid transport. Decomposition of the flow topology into its constituent coherent structures visualises the transport routes and affords insight into the transport properties. The thermal trajectories, by virtue of the fluid-motion analogy, form a thermal topology of essentially equivalent composition. This facilitates heat-transfer visualisation by the same methodology. The thermal topology is defined in both flow and solid regions and thus enables heat-transfer visualisation throughout the entire domain of interest. This offers promising new thermal-analysis capabilities beyond those of conventional methods using temperature and heat-transfer coefficients.

The exposition is organised as follows. Section 2 provides the physical framework for the heat-transfer visualisation in generic unsteady flows. The heat-transfer visualisation is demonstrated for a 3D steady and 2D unsteady flow in Sections 3 and 4, respectively. Conclusions are drawn in Section 5.

2. Heat-transfer visualisation in generic 3D unsteady flows

2.1. Heat transfer in terms of the temperature distribution

Heat transfer in fluid flow is governed by the conservation law for thermal energy, reading

$$\frac{\partial(\rho e)}{\partial t} + \nabla(\rho e \boldsymbol{u}) = q_H - p\nabla\cdot\boldsymbol{u} + \boldsymbol{\sigma} : \nabla\boldsymbol{u} - \nabla\cdot\boldsymbol{q}, \tag{1}$$

with e, ρ and $\boldsymbol{u}$ the internal energy, density and velocity, respectively, of the fluid, q_H a volumetric heat source, p the pressure, $\boldsymbol{\sigma}$ the viscous stress tensor and $\boldsymbol{q}$ the conductive heat flux [5]. The fluid velocity $\boldsymbol{u}$ and pressure p are governed by the well-known conservation laws for mass and momentum [41].

Incompressible flow conditions imply $\rho = \rho(T)$, $e = c_h T$ and $\nabla\cdot\boldsymbol{u} = \beta DT/Dt$, with T the temperature, c_h the specific heat and β the volumetric expansivity [41], and heat conduction generally obeys Fourier's law $\boldsymbol{q} = -\lambda\nabla T$, where λ is the thermal conductivity. Substitution into (1), omitting internal heat sources and viscous heat generation and rescaling variables via $\boldsymbol{x} = L\boldsymbol{x}'$, $\boldsymbol{u} = U\boldsymbol{u}'$, $T = T_{min} + (T_{max} - T_{min})T'$, $p = p_0 p'$, $t = (L/U)t'$ and $\rho = \rho_0\rho'$ yields

$$\frac{\partial(\rho' T')}{\partial t'} + \nabla'(\rho' T' u') = \nabla'\left(Pe^{-1}\nabla' T'\right) - \Pi p' \frac{DT'}{Dt'}, \tag{2}$$

as non-dimensional heat equation. The dimensionless parameters read

$$Pe = \frac{\rho_0 c_h U L}{\lambda}, \Pi = \frac{p_0 \beta}{\rho_0 c_h}, \tag{3}$$

with Pe the well-known Péclet number and Π the non-dimensional thermal expansivity. Here L, U, p_0 and ρ_0 are characteristic length scale, velocity, absolute pressure and density, respectively; $T_{\min}$ and $T_{\max}$ are minimum and maximum temperature within the domain of interest.[2] Quantity $0 \leq T' \leq 1$ represents the non-dimensional temperature fluctuations relative to the uniform background state $T = T_{\min}$. Primes, indicating non-dimensional quantities, are dropped for brevity hereafter.

2.2. Heat transfer in terms of the total heat flux

Thermal expansivity – and thus variation in density – is irrelevant for the heat transfer in the compact systems that motivate the present study.[3] This admits reformulation of (2) into the transport form

$$\frac{\partial T}{\partial t} + \nabla\cdot\boldsymbol{Q} = 0, \quad \boldsymbol{Q} = \boldsymbol{q}_c + \boldsymbol{q}, \quad \boldsymbol{q}_c = T\boldsymbol{u}, \quad \boldsymbol{q} = -\frac{1}{Pe}\nabla T, \tag{4}$$

with $\boldsymbol{q}_c$ and $\boldsymbol{q}$ the convective and conductive heat fluxes, respectively, that combined set up the total heat flux $\boldsymbol{Q}$. (Note that the particular scaling of the temperature, consistent with [7], ensures physical meaningfulness of the convective heat flux $\boldsymbol{q}_c$ in that it is independent of the temperature scale, in the direction of the fluid motion and non-zero only for non-isothermal conditions.) Flux $\boldsymbol{Q}$ delineates the thermal transport routes in an analogous way as the velocity $\boldsymbol{u}$ delineates the transport routes of fluid parcels. This notion forms the backbone of the heat-transfer visualisation proposed in the present study.

2.3. Heat-transfer visualisation

2.3.1. 2D steady conditions

Mass conservation implies for 2D steady conditions a stream function Ψ for the fluid motion, governed by

$$\nabla\cdot\boldsymbol{M} = 0, \quad \boldsymbol{M} = \rho\boldsymbol{u} \Rightarrow \frac{\partial\Psi}{\partial y} = \boldsymbol{M}_x, \quad \frac{\partial\Psi}{\partial x} = -\boldsymbol{M}_y, \tag{5}$$

with $\boldsymbol{M}$ the mass flux. The contours of Ψ delineate the streamlines of the fluid and thus visualise the flow field [41]. Energy conservation (4), analogously, implies a *thermal stream function* Ψ_T, governed by

$$\nabla\cdot\boldsymbol{Q} = 0, \quad \boldsymbol{Q} = T\boldsymbol{u} - Pe^{-1}\nabla T \Rightarrow \frac{\partial\Psi_T}{\partial y} = \boldsymbol{Q}_x, \quad \frac{\partial\Psi_T}{\partial x} = -\boldsymbol{Q}_y, \tag{6}$$

with $\boldsymbol{Q}$ the *total* heat flux defined before. The contours of Ψ_T delineate the "thermal streamlines" (i.e. the paths by which heat transfer occurs) and thus enable heat-transfer visualisation in essentially the same way as flow visualisation by Ψ. This concept has originally been introduced by [28] and has found application in a wide range of studies on 2D steady heat transfer [7,29–35].

2.3.2. Generalisation to 3D unsteady conditions

The contours of the stream function Ψ according to (5) describe the Lagrangian trajectories $\boldsymbol{x}(t)$ of fluid parcels with density ρ in 2D steady flow fields. In generic 3D unsteady flows, these fluid trajectories are governed by

$$\frac{d\boldsymbol{x}}{dt} = \boldsymbol{u}, \quad \frac{\partial\rho}{\partial t} + \nabla(\rho\boldsymbol{u}) = 0. \tag{7}$$

Recasting the heat equation (4) via the identity $\nabla T = T\nabla(\ln T)$ into

$$\frac{\partial T}{\partial t} + \nabla(T\boldsymbol{u}_T) = 0, \quad \boldsymbol{u}_T = \boldsymbol{u} - Pe^{-1}\nabla(\ln T), \tag{8}$$

results in a "continuity constraint" equivalent to that in (7). This has the fundamental implication that generic heat transfer may be represented as the "motion" of "fluid parcels" with "density" T (denoted "heat parcels" henceforth) by the "velocity" $\boldsymbol{u}_T$ subject to continuity and naturally puts forth thermal trajectories $\boldsymbol{x}_T$, governed by

$$\frac{d\boldsymbol{x}_T}{dt} = \boldsymbol{u}_T, \quad \frac{\partial T}{\partial t} + \nabla(T\boldsymbol{u}_T) = 0, \tag{9}$$

as generalisation of the thermal streamlines delineated by Ψ_T to 3D unsteady systems. To date this concept has been restricted to 2D steady flows (Section 2.3.1); first steps towards 3D steady systems are made in [30], directly expanding on formulation (6), and extensions to unsteady conditions are hitherto limited to time-averaged 2D time-periodic flows [30] and weakly-unsteady 2D flows [35]. Formalism (9) constitutes the first unconditional generalisation to generic 3D unsteady heat transfer and paves the way towards one unified Lagrangian methodology for analysis of heat transfer and fluid mixing (generalising that proposed in [31] for 2D steady systems). This is elaborated below.

The continuity constraints in (7) and (9) impose geometrical restrictions upon the fluid and thermal trajectories $\boldsymbol{x}(t)$ and $\boldsymbol{x}_T(t)$, respectively (e.g. they cannot suddenly emerge or terminate inside the flow) and thus organise them into coherent structures that geometrically determine the (thermal) transport properties. The structures formed by $\boldsymbol{x}(t)$ determine the topological make-up ("flow topology") of the web of fluid trajectories [39,42,43]; the thermal trajectories $\boldsymbol{x}_T(t)$, analogously, form a "thermal topology." The flow (thermal) topology is the generalisation of 2D (thermal) streamline portraits to 3D unsteady systems and can be systematically visualised and analysed by well-established geometrical methods from laminar-mixing studies [12,14,37–40]. This approach offers promising new capabilities (e.g. visualisation of thermal transport routes; design of their optimal geometry; in-depth analysis of the still ill-understood link between mixing and efficient heat transfer) beyond those of conventional methods using temperature and heat-transfer coefficients. Its basic concepts and potential are demonstrated hereafter by way of two case studies.

3. Case study I: 3D steady conditions

3.1. Introduction

The heat-transfer visualisation is demonstrated for a basic cooling problem. Considered is a cubical object (side length L) with its hot bottom side maintained at a constant temperature $T_{\max}$ and exposed to a steady incompressible cold fluid flow with uniform inlet velocity U and at uniform inlet temperature $T_{\min}$. The analysis

[2] Note that terms corresponding with the constant contribution $T_{\min}$ to the temperature vanish by virtue of continuity.

[3] Typical characteristics $U \sim \mathcal{O}(0.01\ \mathrm{m/s})$, $L \sim \mathcal{O}(0.01\ \mathrm{m})$, $p_0 \sim \mathcal{O}(10^5\ \mathrm{Pa})$ and fluid properties comparable to those of water readily lead to $Pe \sim \mathcal{O}(100)$ and $\Pi \sim \mathcal{O}(10^{-6})$.

is performed in non-dimensional form (rescaling according to Section 2.1), that is, for a cube with unit side length, unit inlet velocity, inlet temperature $T=0$ and bottom-side temperature $T=1$. The relevant non-dimensional parameters in the 2D/3D cases are

$$Re = \frac{UL}{\nu}, \quad Pe = \frac{UL}{\alpha}, \quad \Lambda = \frac{\lambda_o}{\lambda} = \frac{\alpha_o}{\alpha}, \tag{10}$$

with ν, α and λ the kinematic viscosity, thermal diffusivity and thermal conductivity of the fluid and α_o and λ_o the thermal diffusivity and thermal conductivity of the object. Parameter Re corresponds with the well-known Reynolds number.

The heat transfer in both flow region and object is governed by (4). The former for Pe following (10); the latter for $\boldsymbol{q}_c = 0$ and Pe substituted by $Pe_o = Pe/\Lambda$. Numerical methods for resolution of the 2D/3D flow and temperature fields and the 2D/3D heat-transfer visualisation are furnished in Appendix A.

3.2. 2D steady baseline

Fig. 1 shows the flow and thermal behaviour of the 2D simplification of the cooling problem (flow from left to right) for $Re = 10$, $Pe = 50$ and $\Lambda = 2$. Panel *a* gives the streamline portrait, exposing the flow around the object and the formation of a recirculation zone in its wake and the temperature distribution throughout flow and object. Panel *b* gives the corresponding thermal streamline portrait. The temperature field clearly reflects the cooling of the object by the passing fluid. The thermal streamlines bound, similar to their flow counterparts, adjacent channels that transport thermal energy in the same manner as stream tubes transport fluid and thus are the thermal equivalent to stream tubes.

Continuity dictates that (thermal) stream tubes must either be closed or connect with a boundary (Section 2.3). This implies two kinds of tubes: (i) open tubes connected with (solid) boundaries; (ii) closed tubes. Closed tubes form the "island" that defines the recirculation zone (Fig. 1*a*) entrapping and circulating fluid indefinitely. Open tubes form a "path" that connects inlet and outlet of the flow domain and thus set up net fluid transport.

Thermal stream tubes behave essentially similar. The open tubes inside the object facilitate the heat transfer from its hot bottom side through its interior towards the fluid–solid interface. Here the open thermal stream tubes continue into the flow region and collectively form a "plume" that emerges from the perimeter of the object and rapidly aligns itself with the flow in downstream direction. This plume constitutes the "thermal path" by which heat is removed from the object by the passing fluid. The thermal path is bend around a family of concentric closed thermal stream tubes that collectively form a thermal recirculation zone ("thermal island"). The thermal island entraps and circulates thermal energy and, consequently, forms a thermally-isolated region. The blank region upstream of the thermal path has negligible heat flux ($\boldsymbol{Q} \approx 0$) and, consequently, renders $\boldsymbol{\Psi}_T$ undefined ("thermally-inactive zone"). Thus 2D steady fluid and thermal transport are governed by essentially equivalent coherent structures, viz. (thermal) paths and (thermal) islands, that can be exposed by the (thermal) streamline portraits.

3.3. 3D steady conditions

The continuity constraints here organise the (thermal) streamlines into 3D (thermal) stream tubes with the same key properties as their 2D counterparts: they must either be closed or connect with a boundary. This, similarly as in the 2D case, results in the formation of coherent structures and zones that geometrically determine the (thermal) transport. This is exemplified below by means of the 3D cooling problem.

Fig. 2 shows 3D thermal streamlines $\boldsymbol{x}_T$ according to (9) (vanishing unsteady term in continuity constraint) emanating from the faces of the 3D object at $Re = 10$, $Pe = 100$ and $\Lambda = 2$. (Flow is in x-direction and surface gray scales indicate temperature: dark: $T = 0$; bright: $T = 1$.) These thermal streamlines, as in the 2D case (Fig. 1*b*), delineate the route along which heat is removed from the object by the passing flow and outline the 3D thermal path. This thermal path and a thermally-inactive zone upstream of the object constitute the 3D thermal topology; thermally-isolated (recirculation) zones similar to the thermal island in Fig. 1*b* are absent in this particular case. The thermal topology of the 3D cooling problem thus is of similar composition as that of its 2D simplification. Central entity in both 2D and 3D cases is the thermal path by which the actual cooling of the object happens. Thermal paths in fact *always* form in the presence of non-adiabatic walls and their (geometrical) properties are key to fluid-wall heat exchange as well as net thermal transport within the flow in *any* configuration [36].

Essential difference between 2D and 3D steady topologies is that the latter may exhibit far greater topological complexity [39,44]. Thermally-isolated zones may in 3D steady topologies e.g. emerge in a form similar to tubular non-mixing zones (i.e. the 3D generalisation of islands) or spheroidal transport barriers known

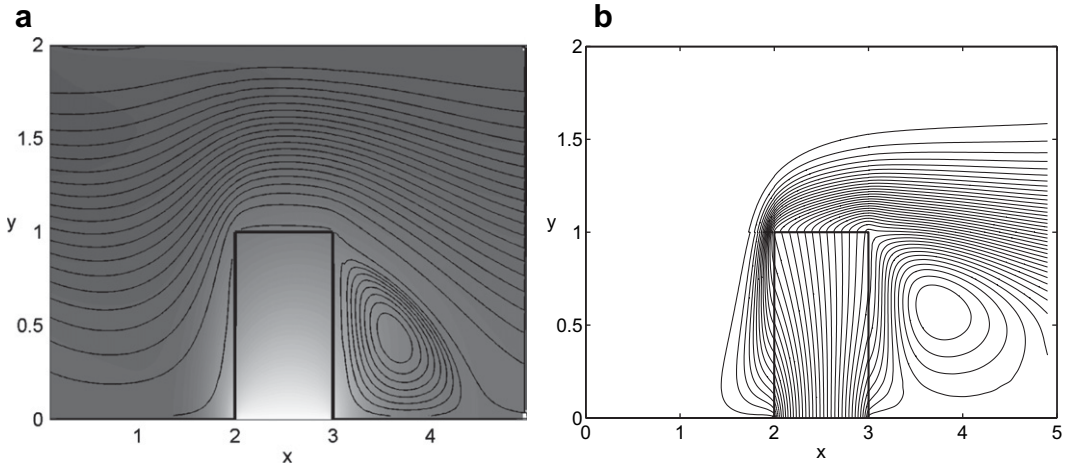

Fig. 1. 2D cooling problem for $Re = 10$, $Pe = 50$, $\Lambda = 2$. Panel *a* shows the fluid streamlines and temperature (dark: $T = 0$; bright: $T = 1$); panel *b* shows thermal streamlines.

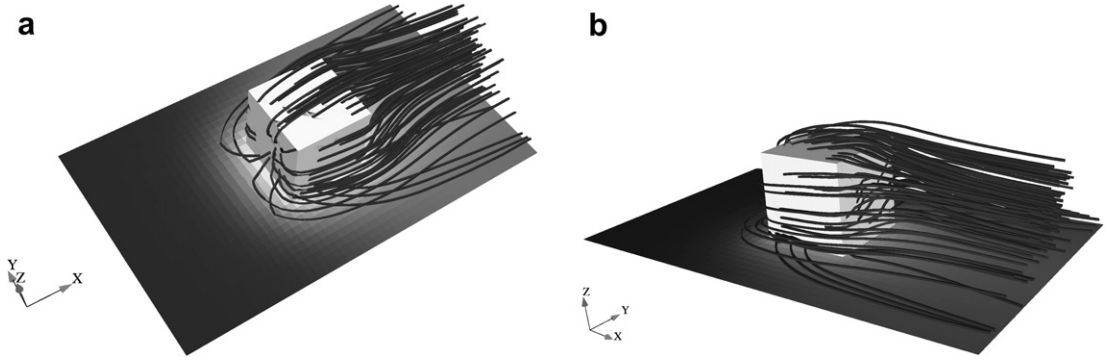

Fig. 2. 3D thermal path emanating from the hot object for $Re = 10$, $Pe = 100$ and $\Lambda = 2$. The outline of the thermal path is visualised by 3D thermal streamlines originating from the faces of the object. Flow is in negative x-direction; surface gray scales indicate temperature (dark: $T = 0$; bright: $T = 1$).

from 3D steady mixing flows [40,45]. Moreover, 3D thermal streamlines may become chaotic and thus give rise to chaotic transport of heat parcels mechanistically equivalent to chaotic advection of fluid parcels in 3D steady flows [14,40,45,46]. The connection between chaotic fluid advection and (chaotic) heat transfer is in fact of great practical relevance and, consequently, the subject of investigation in many studies [2,23–27,47]. This important issue is pursued further in terms of a representative 2D unsteady system – to which 3D steady systems are dynamically equivalent [45] – hereafter.

4. Case study II: 2D unsteady conditions

4.1. Introduction

Heat-transfer visualisation in unsteady flows is demonstrated for a non-dimensional heat-transfer problem within the 2D domain $(x, y) = [0, 1] \times [0, 1/2]$ with spatially-periodic inlet ($x = 0$) and outlet ($x = 1$) and solid bottom ($y = 0$) and top ($y = 1/2$) walls. Heat transfer is induced via the "hot" isothermal bottom (temperature $T = 1$) wall and "cold" isothermal top wall ($T = 0$). The heat transfer is governed by the non-dimensional heat equation (4), with time-periodic flow field $\boldsymbol{u}(\boldsymbol{x}, t) = \overline{\boldsymbol{u}}(\boldsymbol{x}_+, t) + \overline{\boldsymbol{u}}(\boldsymbol{x}_-, t) = \boldsymbol{u}(\boldsymbol{x}, t + 1)$ (period time $\tau = 1$) set up by two adjacent vortices centred at $\boldsymbol{x}_+ = (1/4 - \Delta x(t), 1/4)$ (counter-clockwise rotation) and $\boldsymbol{x}_- = (3/4 - \Delta x(t), 1/4)$ (clockwise rotation), respectively. The solenoidal velocity field $\overline{\boldsymbol{u}}$ is given analytically by

$$\overline{u}_x(x, y) = \sin(2\pi x)\cos(2\pi y), \quad \overline{u}_y(x, y) = -\cos(2\pi x)\sin(2\pi y) \tag{11}$$

and $\Delta x(t) = \Delta x(t + 1) = \epsilon \sin(2\pi t)$ is the horizontal time-periodic oscillation of the vortex pair with amplitude ϵ. System parameters are the Péclet number Pe introduced before and the amplitude ϵ. Numerical methods for resolution of the temperature field and the 2D heat-transfer visualisation are in Appendix B.

4.2. 2D steady baseline

Fig. 3*a* gives the streamline portrait $\boldsymbol{\Psi}$ and temperature field at $Pe = 10$ for steady conditions ($\epsilon = 0$), comprising two adjacent islands, each associated with one vortex (left: counter-clockwise circulation; right: clockwise circulation). Fig. 3*b* gives the corresponding thermal streamlines, clearly revealing the thermal path, connecting the non-adiabatic bottom and top walls and sandwiched in between two thermal islands. The wide sections of the thermal path that attach to the non-adiabatic walls coincide with the thermal boundary layers; the contraction occurs in the internal flow outside these layers.

The streamline portrait consists entirely of islands; paths connecting boundaries are, unlike the cooling problem considered before, absent here. This is a direct consequence of the fact that the domain is bounded by solid walls impermeable to fluid. The streamline portraits of closed 2D steady flows as that considered here are organised by two types of stagnation points: (i) elliptic

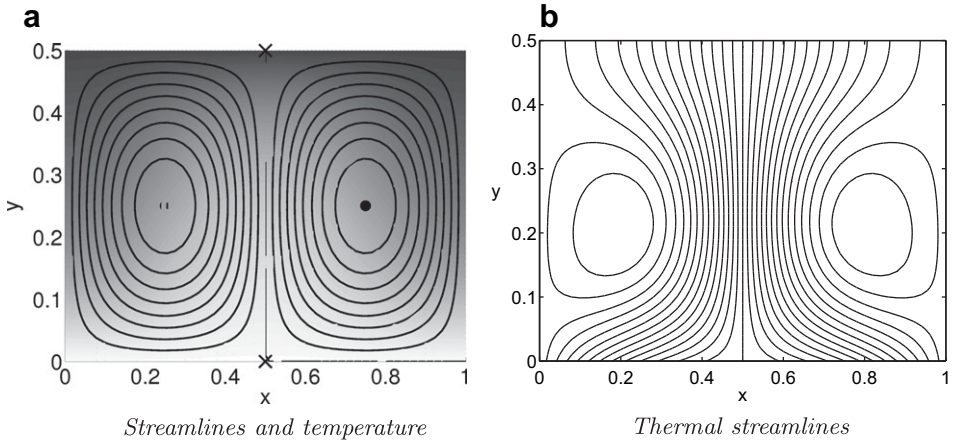

Fig. 3. Steady vortex flow ($\epsilon = 0$) for $Pe = 10$. Panel *a* gives the streamline portrait and the typical temperature field (dark: $T = 0$; bright: $T = 1$); panel *b* gives the thermal streamline portrait.

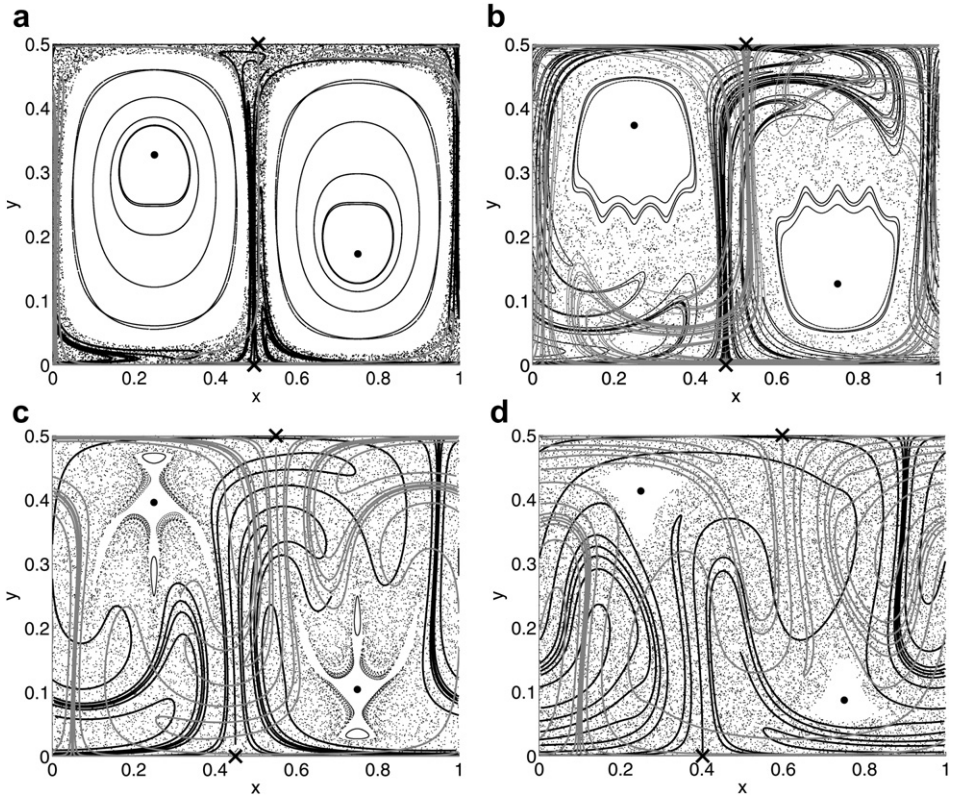

Fig. 4. Progression of the flow topology with increasing time-periodic fluctuation ϵ (=0.01, 0.05, 0.1, 0.2) visualised by the Poincaré-section (dots) of an array of fluid parcels released on $y = 1/4$. Large black dots and black crosses indicate elliptic and hyperbolic periodic points, respectively; gray and black curves indicate stable and unstable manifolds, respectively, of the hyperbolic points.

points (centres of islands); (ii) hyperbolic points (origin of separatrices of islands) [42,48].[4] The former and latter type are both present in Fig. 3*a* and are indicated by the dots and crosses, respectively. The thermal streamline portrait, on the other hand, is only partially organised by stagnation points, since the domain is non-closed in thermal sense by virtue of the non-adiabatic walls. Here only elliptic stagnation points emerge, viz. the centres of the thermal islands in Fig. 3*b*. The remainder of the thermal streamline portrait consists of the thermal path, the existence of which is, as before, inextricably linked with the presence of non-adiabatic walls [36].

4.3. Unsteady conditions

4.3.1. Fluid motion

The fluid motion can in time-periodic flows be visualised by so-called Poincaré-sections. These are in essence stroboscopic "illuminations" of the fluid parcels after each period and thus correspond with the string of subsequent parcel positions at the discrete time levels $t \in [0,\tau,2\tau,\ldots]$, with $\tau = 1$ the period time introduced before [42,46]. The Poincaré-sections of fluid parcels released at "strategic" locations visualise the flow topology in a manner akin to the streamline portraits in steady flows. Fig. 4 shows the Poincaré-sections (black dots) of an array of fluid parcels released on the line $y = 1/4$ for growing time-periodicity, comprising islands embedded in a chaotic sea that expand with increasing ϵ. This is the progression from the regular steady state towards a fully chaotic state well-known from 2D mixing flows [14,37,42,46].

The Poincaré-section of closed time-periodic flows is organised by periodic points and associated coherent structures. Periodic points are the time-periodic equivalent to stagnation points and correspond with material points that periodically return to their initial position (period-p points return after p cycles). 2D time-periodic flows governed by (7) admit, in analogy with the stagnation points, two types: elliptic and hyperbolic points [42,46]. Elliptic points form the centres of islands in the Poincaré-sections (large dots in Fig. 4).

Hyperbolic points (crosses in Fig. 4) are the origin of so-called manifolds (black and gray curves in Fig. 4) that occupy (and create) the chaotic sea. These manifolds are the time-periodic analogy to separatrices in steady flows and delineate the principal transport directions in the chaotic sea [14,42,46]. Gray ("stable") and black ("unstable") manifolds correspond with transport to and from the hyperbolic point, respectively. Manifolds, unlike separatrices, can intersect outside their underlying (periodic) points, however. This effectuates exponential stretching of fluid parcels and is the key mechanism behind chaotic fluid transport; manifold-interaction zones thus are synonymous to chaotic-advection (or "efficient mixing") zones [14,37,42,46].

The chaotic sea ensues from the break-up of the steady-state islands by mechanisms well-known from 2D dynamical systems. For "weak" time-periodicity ("low" ϵ) the break-up scenario is according to the classical KAM/Poincaré–Birkhof theorems [42,46]; for "strong" time-periodicity ("high" ϵ) the system may undergo nonlinear bifurcations that promote further disintegration of the (remants of the) islands – and thus further "chaotisation" of the transport [46].

[4] The streamline portrait of the 2D cooling problem in Section 3 is only partially organised by stagnation points, namely the recirculation zone centred on an elliptic stagnation point in the wake of the object.

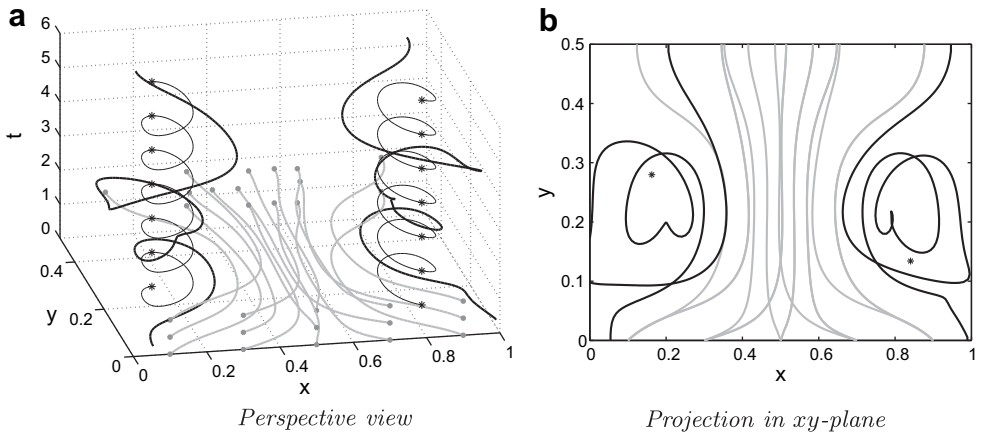

Fig. 5. Typical arrangement of thermal trajectories in the time-space domain ($Pe = 10$ and $\epsilon = 0.05$). Panel *a* gives the perspective view; panel *b* gives the projection in the *xy*-plane. Stars indicate elliptic periodic points; thin curves in panel *a* delineate the corresponding orbit. Thick gray and black curves indicate non-coiled and coiled trajectories, respectively.

4.3.2. Heat transfer

The thermal transport also admits visualisation in terms of Poincaré-sections. However, similar as in the steady case, the system is open in thermal sense, meaning that heat parcels on a given thermal trajectory may exit the domain before leaving a clear footprint in the Poincaré-section. Thus Poincaré-sections alone generally provide insufficient insight into the heat transfer. Therefore, for heat-transfer visualisation both Poincaré-sectioning and visualisation of the thermal trajectories in the time-space domain is employed.

Fig. 5 shows a typical arrangement of thermal trajectories in the time-space domain, demonstrated for $Pe = 10$ and $\epsilon = 0.05$, in perspective view (panel *a*) and projected into the *xy*-plane (panel *b*). Stars indicate elliptic periodic points and the thin curves in panel *a* delineate the corresponding orbit. Two kinds of thermal trajectories can be distinguished: (i) non-coiled trajectories (thick gray

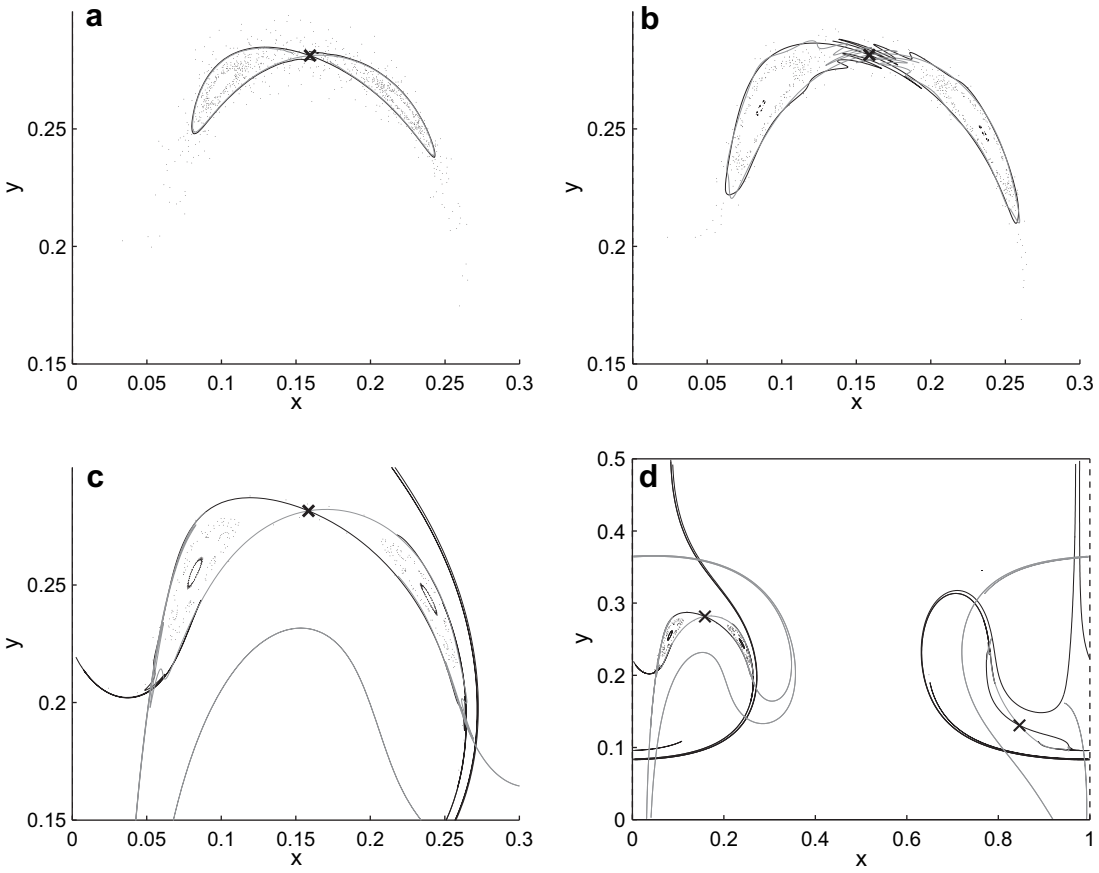

Fig. 6. Onset to chaotic heat transfer by period-doubling bifurcation of the elliptic points of the thermal islands demonstrated for $Pe = 10$ (hyperbolic point: star; period-2 islands: Poincaré-sections). Panels *a–c* give the progression of the local thermal topology and expansion of the manifold-interaction zone (panel c) with increasing ϵ (=0.0550, 0.0560, 0.0563); panel *d* shows the spatial extent – and attachment to the non-adiabatic walls – of the expanded manifolds.

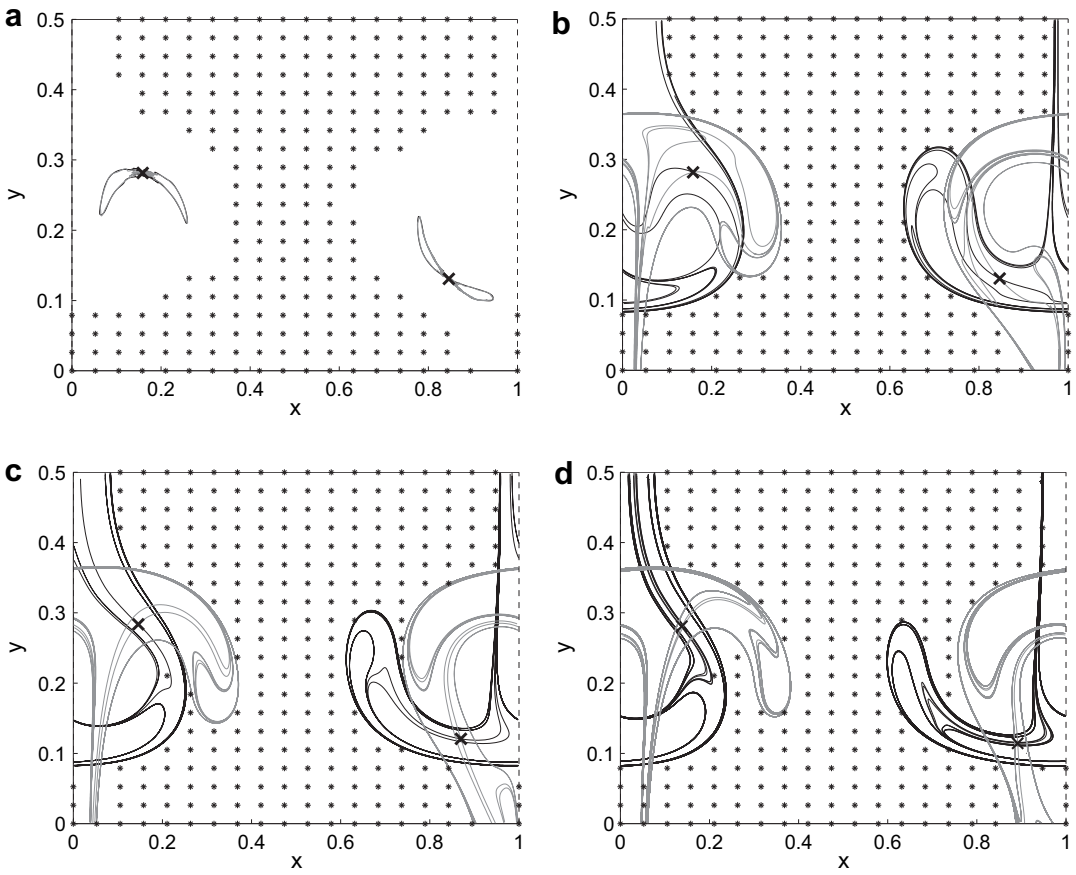

Fig. 7. Chaotisation of heat transfer through expansion of the manifold-interaction zone with increasing time-periodicity ϵ (=0.0560, 0.0565, 0.08, 0.1) at $Pe = 10$. Shown are the hyperbolic points (crosses) and associated stable (gray curves) and unstable (black curves) manifolds (chaotic heat transfer) and the region occupied by non-coiled thermal trajectories (regular heat transfer; stars).

curves); (ii) coiled trajectories (thick black curves).[5] The former directly connect the non-adiabatic bottom and top walls and form open thermal stream tubes in the time-space domain that set up heat exchange between bottom and top walls in the same way as the steady-state thermal path (Fig. 3*b–d*). The latter stem from progressive disintegration of the steady-state thermal island with increasing time-periodicity by which its closed thermal trajectories generically become non-closed. This non-closedness dictates that the coiled trajectories, similar to non-closed (thermal) streamlines in steady systems, must connect with non-adiabatic boundaries and thus also form open thermal stream tubes in the time-space domain, albeit of far greater topological complexity than their non-coiled counterparts [36]. Hence, the thermal path consists of both non-coiled and coiled thermal trajectories. Reminiscent of the steady baseline, periodic points only partially organise the thermal topology, viz. the part emanating from the thermal island. This part undergoes transition to chaos and thus underlies the occurrence of chaotic heat transfer – or efficient "thermal mixing" in the present fluid-motion analogy. This is elaborated below.

Disintegration of the thermal island – and the inherent chaotisation of the (spatio-temporal) thermal stream tubes – results from essentially the same mechanisms as those underlying disintegration of islands in 2D mixing flows (Fig. 4). The break-up at "weak" time-periodicity ("low" ϵ) follows the same scenario as that for the islands in the flow topology, implying persistent thermal islands centred on the elliptic points (reminiscent of the islands in Fig. 4) around which the thermal trajectories coil up. This coiling up is weakly-chaotic due to the formation of (localised) chaotic seas in the break-up region of the thermal island. Hence the somewhat erratic and asymmetric winding patterns of the coiled thermal trajectories in Fig. 5.

For "stronger" time-periodicity ("higher" ϵ) both period-1 elliptic points undergo a so-called period-doubling bifurcation (here at $\epsilon \approx 0.054$): each elliptic point transforms into a hyperbolic point under the formation of two adjacent period-2 elliptic points [46]. This signifies the onset to chaotic heat transfer and is demonstrated in Fig. 6 for $Pe = 10$. Panel *a* gives the situation just after the bifurcation; shown are the period-1 hyperbolic point (star) and its manifolds encircling two period-2 islands (visualised by Poincaré-sectioning). Stable (gray) and unstable (black) manifolds interact only weakly here and are therefore nearly indistinguishable. Increasing the time-periodicity intensifies the manifold interaction and expands the associated chaotic sea at the cost of the islands (panel *b*). The manifold-interaction zone remains localised, though. Slightly stronger time-periodicity ($\epsilon \approx 0.0563$) causes sudden extension of the manifolds from this zone (panel *c*) into a region roughly coinciding with the steady-state thermal island (panel *d*). The stable and unstable manifolds, by virtue of continuity, attach to the bottom and top walls, respectively, and thus set up chaotic heat exchange between these walls via the flow.

Fig. 7 demonstrates the heat-transfer chaotisation with increasing time-periodicity for the full domain. Two kinds of

[5] Thermal trajectories crossing $y = 1/4$ once are denoted "non-coiled," otherwise "coiled".

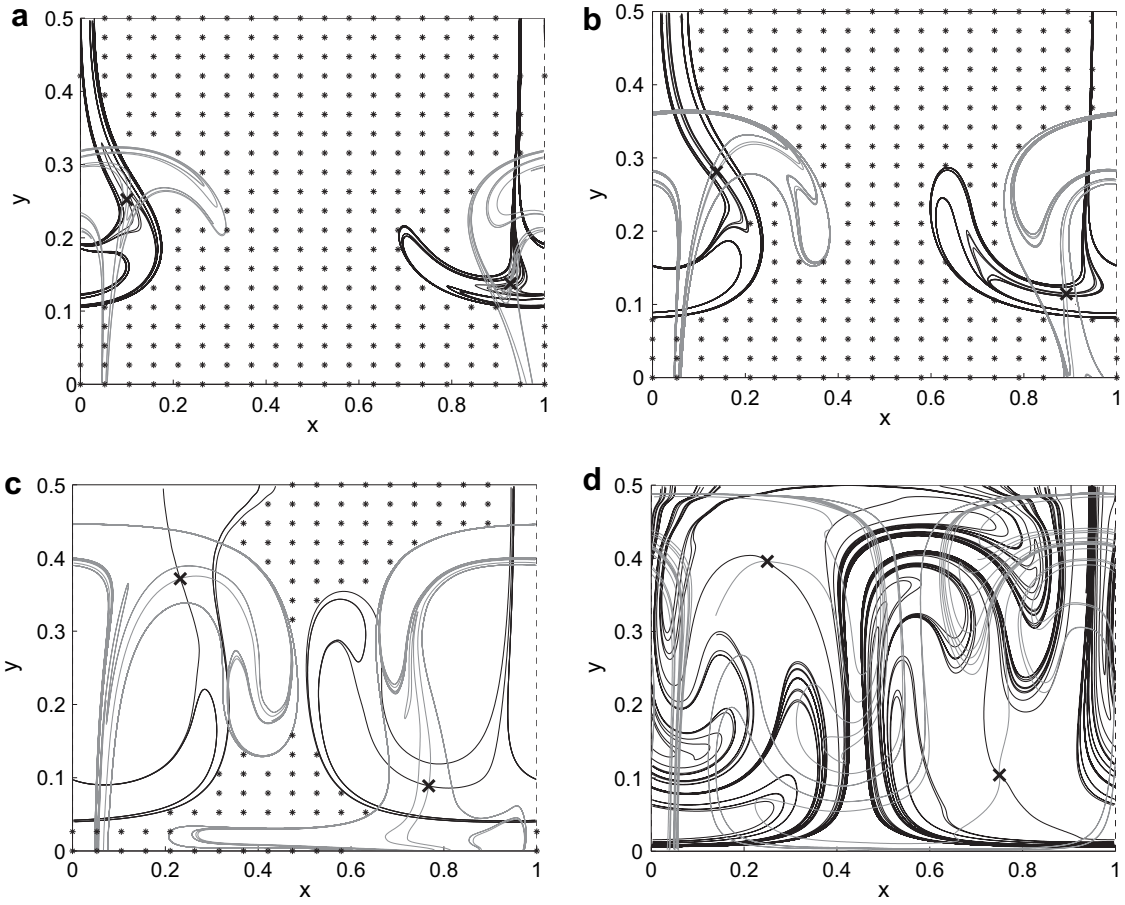

Fig. 8. Connection between chaotic advection and the occurrence of chaotic heat transfer demonstrated for $\epsilon = 0.1$ and $Pe = 7, 10, 50, 1000$. Shown are the hyperbolic points (crosses) and associated stable (gray curves) and unstable (black curves) manifolds (chaotic heat transfer) and the region occupied by non-coiled thermal trajectories (regular heat transfer; stars).

coherent structures are relevant in this regard. First, the manifold-interaction zones associated with the hyperbolic points (crosses) originating from the above bifurcations, signifying chaotic heat transfer. Second, the region(s) occupied by non-coiled thermal trajectories (stars), signifying regular heat transfer.[6] Both manifold-interaction zones remain localised and embedded in a weakly-chaotic sea (blank region) up to $\epsilon \approx 0.056$ (panel *a*) and rather abruptly expand and attach to the bottom and top walls for marginally stronger time-periodicity (panel *b*). The zones remain separated by the non-coiled trajectories during this expansion, however. Further increasing the time-periodicity brings about but minor changes in the thermal topology (panels *c* and *d*). Attachment of the manifolds to the non-adiabatic walls implies that the chaotic zones become part of the thermal path. Thus beyond a threshold for ϵ (here $\epsilon \approx 0.056$) the thermal path comprises two parts: (i) regular part formed by the non-coiled thermal trajectories; (ii) chaotic part formed by the manifold-interaction zones. The latter are the thermal equivalent to efficient mixing zones, denoted "thermal-mixing zones" hereafter, and their spatial extent – and thus the degree of chaotic heat transfer – depends essentially on *Pe*. This is considered below.

The connection between efficient thermal mixing – and its effect upon fluid-wall heat transfer – and efficient fluid mixing (i.e. chaotic advection) has, owing to its practical relevance, been investigated in many studies [2,23–27,47]. However, these studies consider this only indirectly in terms of temperature distributions and heat-transfer coefficients at solid walls. The present Lagrangian approach facilitates visualisation of (possible) thermal-mixing zones and thus enables a more direct correlation with fluid-mixing zones. Simulations reveal that, on the one hand, fluid mixing is imperative for the occurrence of thermal mixing yet, on the other hand, their connection is highly non-trivial and depends essentially on *Pe*. Increasing *Pe* causes, similar to the foregoing steady cases, progression of the thermal topology towards its convection-dominated state; thermal-mixing and fluid-mixing zones thus approach one another with growing *Pe*. Conversely, the thermal-mixing zones diminish with decreasing *Pe* (signifying regularisation of heat transfer) and vanish altogether below a given threshold ($Pe_{\min}$) for *Pe* in favour of thermal islands. This expansion of thermal-mixing zones with increasing convection – and, conversely, the regularisation of heat transfer by conduction – is demonstrated in Fig. 8 for $\epsilon = 0.1$. Comparison of shown thermal topologies with the corresponding flow topology (Fig. 4*c*) clearly reveals that fluid-mixing and thermal-mixing zones deviate progressively with decreasing *Pe*. This underscores the highly non-trivial connection between (chaotic) fluid and heat transfer in cases with significant conduction. The onset to (local) thermal mixing by break-up of thermal islands upon exceeding $Pe > Pe_{\min}$ occurs through the same

[6] The (approximate) region occupied by non-coiled thermal trajectories is outlined by determining which thermal trajectories emanating from an equidistant grid of tracers covering the entire domain and released at $t = 0$ are non-coiled.

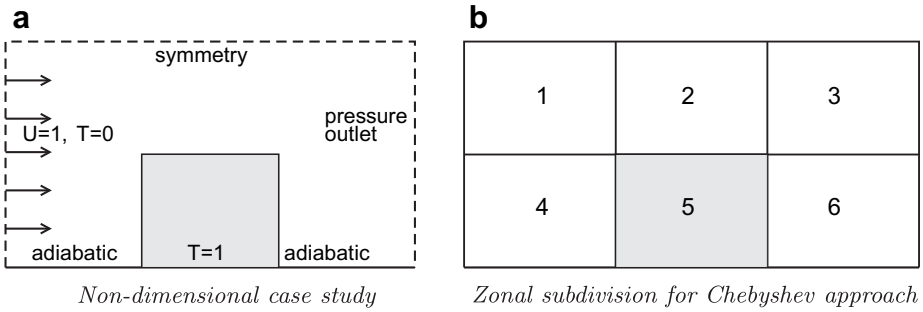

Fig. A.9. Numerical treatment case study I. Panel *a* shows the non-dimensional configuration including (thermal) boundary conditions (essentially similar for 2D and 3D cases); panel *b* shows the subdivision of the 2D domain into rectangular zones for the numerical treatment with the Chebyshev expansion (A.1).

mechanism as before, viz. a period-doubling bifurcation of the elliptic periodic points associated with said islands. Thus convection must be sufficiently dominant ($Pe > Pe_{\min}$) as well as sufficiently chaotic ($\epsilon > \epsilon_{\min}$) for thermal mixing to happen.

4.4. Towards generic 3D unsteady systems

Heat-transfer visualisation in generic 3D unsteady systems is in essence similar to that demonstrated above for 2D time-periodic systems. The thermal trajectories $\boldsymbol{x}_T$ remain governed by relations (9) and 3D heat-transfer visualisation can basically adopt the same methods: 3D Poincaré-sections and representations in the 4D time-space domain. Moreover, non-periodic systems admit visualisation in terms of "wandering" hyperbolic points and associated manifolds; these constitute the non-periodic counterparts to hyperbolic points and manifolds in time-periodic systems [38,49].

However, 3D unsteady heat-transfer visualisation, despite resting on the same concepts and methods, is complicated significantly on grounds of the far greater topological complexity relative to 2D unsteady and 3D steady systems [39,44,50] and, consequently, the absence of a fully-developed theoretical framework. The flow and thermal topologies of time-periodic systems are e.g. organised by periodic lines and isolated periodic points, the associated coherent structures of which may form intricate spatial arrangements that are difficult to visualise in an insightful and systematic manner; the theory on "wandering" hyperbolic points is hitherto restricted to highly-idealised 2D systems [38,49]. Moreover, the scenarios and mechanisms underlying 3D chaotic (heat) transport are largely unexplored to date and subject of ongoing research [51–54].

5. Conclusions

The study considers heat transfer as the transport of thermal energy by the *total* convective–conductive heat flux in a way analogous to the transport of fluid by the flow field. This facilitate heat-transfer visualisation in a similar manner as flow visualisation and has great potential for analysis of thermal systems. To date this unified concept has been restricted to 2D steady flows. The present study proposes its generalisation to 3D unsteady flows.

Continuity organises fluid trajectories into coherent structures (defining the flow topology) that geometrically determine fluid transport. Decomposition of the flow topology into these coherent structures by geometrical methods well-known from laminar-mixing studies visualises the transport routes and affords insight into the transport properties. The thermal trajectories, by virtue of the fluid-motion analogy, form a thermal topology that is of essentially equivalent composition. This facilitates heat-transfer visualisation by the same geometrical methodology and has been demonstrated by way of examples.

Fluid and heat transfer in 2D steady systems is determined by (thermal) streamline portraits that are composed of two kinds of coherent structures: (i) (thermal) islands that entrap and circulate fluid or heat; (ii) (thermal) paths attached to boundaries that set up net fluid or heat transport. 3D steady systems behave similarly in that 3D (thermal) stream tubes form with similar properties as their 2D counterparts. Thermal paths are key to fluid-wall heat exchange and net thermal transport within the flow in both 2D and 3D systems. However, the 3D flow and thermal topologies may exhibit greater topological complexity and in principle admit chaotic fluid and heat transfer.

2D time-periodic flows also admit chaotic fluid and heat transfer. This manifests itself in the (partial) break-up of (thermal) islands into chaotic seas and in the "chaotisation" of the thermal path – and thus the heat transfer *in toto* by scenarios well-known from laminar mixing. The chaotic seas form "thermal-mixing zones" and are the thermal equivalent to efficient fluid-mixing zones. The proposed approach thus facilitates in-depth investigation of the (still ill-understood) connection between chaotic heat transfer and chaotic mixing.

Unified flow and heat-transfer visualisation in 3D unsteady systems is in essence similar to that demonstrated for 2D unsteady systems in that 3D topologies remain governed by the same relations. However, they may exhibit far greater topological complexity. Moreover, the scenarios and mechanisms underlying the onset to 3D chaotic (heat) transport are largely unexplored to date. Further development of the unified topological framework for transport in 3D unsteady systems and its applications to fluid and heat transfer is in progress.

Appendix A. Numerical methods: case study I

Resolution of flow and temperature fields

Numerical simulation of the governing 2D/3D conservation laws are carried out with the commercial finite-volume method (FVM) package Fluent using boundary conditions according to Fig. A.9*a*. (Conditions for 2D and 3D case are in essence the same.) This facilitates efficient resolution of the flow and temperature fields in the complex domain comprising flow and solid regions and discontinuous boundaries.

2D interpolation

The velocity and temperature fields are approximated by Chebyshev expansions [55]. This admits substantial reduction of the data sets – and thus of the computational effort required for data processing – compared to the FVM data sets due to the exponential

convergence of the Chebyshev spectrum. Representation in Chebyshev polynomials furthermore facilitates easy and accurate evaluation of derived quantities. Key condition for exponential convergence is that fields be sufficiently smooth, however. To this end the flow domain is subdivided into six rectangular zones (Fig. A.9*b*) within which this smoothness constraint is met. The fields are in each of these zones expanded as

$$f(x,y) = \sum_{m=0}^{M}\sum_{n=0}^{N}\widehat{f}_{nm}\phi_m(\eta(x))\phi_n(\zeta(y)), \tag{A.1}$$

with $\phi_k(z) = \cos(k \arccos z)$ the k-th order Chebyshev polynomial, defined on the interval $-1 \le z \le 1$, and

$$\eta = \frac{2x-(X_1+X_0)}{X_1-X_0}, \quad \zeta = \frac{2y-(Y_1+Y_0)}{Y_1-Y_0}, \tag{A.2}$$

linear mappings of the physical domain onto the computational domain, where (X_0, X_1) (Y_0, Y_1) demarcate the bounds of the rectangular region in question (Fig. A.9*b*). The spectral coefficients $\widehat{f}_{nm}$ are evaluated via discrete Chebyshev transforms [55] by interpolation of the Fluent data onto the Chebyshev grid with the built-in routine griddata of the commercial high-level programming language Matlab. This yields the matrix with spectral coefficients $\boldsymbol{F}$, the entries of which are given by $(\boldsymbol{F})_{nm} = \widehat{f}_{nm}$, where columns and rows correspond with the $x-$ wise and $y-$ wise expansions, respectively.

3D interpolation

In the 3D configuration the above spectral approach becomes impracticable. Here interpolation of FVM data as well as derived quantities is therefore based entirely upon the built-in Matlab routine griddata3.

Computation of 2D gradients

The spectral approximation of the gradient $\boldsymbol{g} = \nabla f$ of 2D functions $f(x,y)$ according to (A.1) follows readily from application of the relations for first derivatives of Chebyshev expansions and reads

$$\boldsymbol{G}_x = \frac{2}{X_1-X_0}\boldsymbol{F}\cdot\boldsymbol{D}^T(M), \quad \boldsymbol{G}_y = \frac{2}{Y_1-Y_0}\boldsymbol{D}(N)\cdot\boldsymbol{F}, \tag{A.3}$$

with $(\boldsymbol{D}(K))_{ij} = 2j/c_i$ for $i+j$ *odd* and $j>i$ and $(\boldsymbol{D}(K))_{ij} = 0$ otherwise [55]. Here $c_i = 2$ and $c_i = 1$ for $i = 0$ and $i > 0$, respectively, where $0 \le i, j \le K$. Important to note is that this approach enables *exact* evaluation of the gradient of the Chebyshev expansion (A.1) [55]. Hence, approximation errors of the FVM data are induced solely by their interpolation onto said expansion. This absence of additional approximation errors in derived quantities is a key advantage of the adopted approach over conventional methods as e.g. finite-difference schemes.

Computation of 3D gradients

3D gradients are evaluated on the Fluent grid $\boldsymbol{x}_F$ via a standard central-difference scheme

$$g_x(\boldsymbol{x}_F) = \frac{f(x_F+\Delta x, y_F, z_F)-f(x_F-\Delta x, y_F, z_F)}{2\Delta x}, \tag{A.4}$$

and likewise for $\boldsymbol{g}_{y,z}$. (Backward/forward-difference schemes are employed in case $\boldsymbol{x}_F$ coincides with domain boundaries.) The required interpolation of scalar f to adjacent positions is performed by the built-in Matlab routine griddata3.

Computation of 2D (thermal) stream functions

The 2D (thermal) stream functions follow from inversion of the gradient operator: $h = \nabla^{-1}\boldsymbol{g}$, where $(h, g_x, g_y) = (\Psi, -M_y, M_x)$ (fluid) or $(h, g_x, g_y) = (\Psi_T, -Q_y, Q_x)$ (heat). This embarks on individually inverting the matrix relations in (A.3), i.e.

$$\boldsymbol{H}^{(x)} = \frac{X_1-X_0}{2}\boldsymbol{G}_x\cdot\overline{\boldsymbol{D}}^{-T}(M), \quad \boldsymbol{H}^{(y)} = \frac{Y_1-Y_0}{2}\overline{\boldsymbol{D}}^{-1}(N)\cdot\boldsymbol{G}_y, \tag{A.5}$$

with $\overline{\boldsymbol{D}}$ the regularised first-derivative matrix $\boldsymbol{D}$ (the last element in the first column is set to unity). Matrices $\boldsymbol{H}^{(x)}$ and $\boldsymbol{H}^{(y)}$ identify with the sought-after matrix $\boldsymbol{H}$ up to the first columns and rows, respectively. This straightforwardly leads to $\boldsymbol{H} = [\boldsymbol{h}_0^{(y)}\boldsymbol{h}_1^{(x)}\ldots\boldsymbol{h}_M^{(x)}]$, with $\boldsymbol{h}_k^{(x,y)}$ the k-th column vector of matrix $\boldsymbol{H}^{(x,y)}$. This approach determines the spectrum $\boldsymbol{H}$ entirely, save the constant $\widehat{H}_{00}$, which can be chosen arbitrarily.

Computation of 3D (thermal) streamlines

Trajectories $\boldsymbol{x}(t)$ corresponding with a 3D steady vector field $\boldsymbol{v}(\boldsymbol{x})$ are governed by the kinematic equation $d\boldsymbol{x}/dt = \boldsymbol{v}$. Numerical integration with a third-order Taylor–Galerkin scheme results in the time-marching scheme

$$\boldsymbol{x}_{n+\frac{1}{3}} = \boldsymbol{x}_n + \frac{\Delta t}{3}\boldsymbol{v}(\boldsymbol{x}_n), x_{n+\frac{1}{2}} = \boldsymbol{x}_n + \frac{\Delta t}{2}\boldsymbol{v}\left(\boldsymbol{x}_{n+\frac{1}{3}}\right),$$
$$\boldsymbol{x}_{n+1} = \boldsymbol{x}_n + \Delta t\boldsymbol{v}(\boldsymbol{x}_n),$$

with $t_k = k\Delta t$ the discrete time levels and $\boldsymbol{x}_k$ the corresponding position [55].

Appendix B. Numerical methods: case study II

Resolution of temperature field

The temperature field is simulated by numerical resolution of the standard advection-diffusion form of the energy equation (4), with an analytical flow field according to (11) via a conventional Fourier-Chebyshev spectral method in combination with a second-order Crank–Nicholson time-marching scheme [55]. This ansatz affords great precision and leans on Fourier–Chebyshev expansion of variables according to

$$f(x,y,t) = \sum_{m=-M/2}^{M/2-1}\sum_{n=0}^{N}\tilde{f}_{nm}(t)\psi_m(x)\phi_n(\zeta(y)), \tag{B.1}$$

with $\psi_m = \exp(i\pi x)$ the m-th order Fourier polynomial and ϕ_n the n-th order Chebyshev polynomial defined before, where $Y_0 = 0$ and $Y_1 = 1/2$ in the mapping $\zeta(y)$. The spectrum of the analytical flow field follows from discrete Fourier–Chebyshev transforms; the spectral solver simulates the time-evolution of the spectrum of the temperature field. Thermal conditions on the adiabatic sidewalls are met automatically by expansion (B.1); thermal conditions on the non-adiabatic walls are implemented via the standard Lanczos tau method [55].

Interpolation and computation/inversion of gradients

Interpolation is readily performed with the Fourier–Chebyshev expansion (B.1) and gradients of scalar quantities are computed from the associated spectra in essentially the same way as for the above 2D Chebyshev expansion on grounds of the similarity between Fourier and Chebyshev expansions [55]. The (thermal) stream functions follow via inversion of the discrete gradient operator also in basically the same manner. This approach, as

before, enables *exact* evaluation of gradients of variables expressed as expansion (B.1).

Computation of unsteady (thermal) trajectories

This employs the 2D version of the Taylor–Galerkin scheme (5) incorporating explicit time dependence of the vector field $\boldsymbol{v}$.

Isolation and tracking of material points and curves

Periodic points correspond with material points in time-periodic (thermal) flow fields that return to their initial position after a given number of cycles. These points are identified by isolation of common roots $dX = dY = 0$ of the displacement functions $dX(\boldsymbol{x})$ and $dY(\boldsymbol{x})$, with (dX, dY) the displacement of the material point $\boldsymbol{x}$ after one period, by a 2D simplification of the dedicated 3D root-finding algorithm by [50]. Their type (i.e. elliptic or hyperbolic) is determined by the numerical approach following [56]. The manifolds of hyperbolic periodic points are material curves that are tracked by a 2D version of the 3D front-tracking algorithms by [50].

References

[1] M.F. Edwards, Heat transfer in in-line static mixers. in: S. Kakac, R.K. Shah, A.E. Bergles (Eds.), Low Reynolds Number Flow Heat Exchangers. Springer, Berlin, 1983, p. 783.
[2] D.R. Lester, M. Rudman, G. Metcalfe, Low Reynolds number scalar transport enhancement in viscous and non-Newtonian fluids. Int. J. Heat Mass Transf 52 (2008) 655.
[3] S. Cerbelli, V. Vitacolonna, A. Adrover, M. Giona, Eigenvalue-eigenfunction analysis of infinitely fast reactions and micromixing regimes in regular and chaotic bounded flows. Chem. Eng. Sci. 59 (2004) 2125.
[4] W. Liu, G. Haller, Strange eigenmodes and decay of variance in the mixing of diffusive tracers. Physica D 188 (2004) 1.
[5] M. Kaviany, Principles of Convective Heat Transfer. Springer, New York, 2001.
[6] R.K. Shah, D.P. Sekulić, Fundamentals of Heat Exchanger Design. Wiley, Chichester, 2003.
[7] A. Bejan, Convection Heat Transfer. Wiley, New York, 1995.
[8] B. Sundén, R.K. Shah, Advances in Compact Heat Exchangers. Edwards, Philadelphia, 2007.
[9] D. Reay, Learning from Experiences with Compact Heat Exchangers CADDET Analysis Series 25. CADDET, Sittard, 1999.
[10] Y. Jaluria, Thermal processing of materials: from basic research to engineering. ASME J. Heat Transf 125 (2003) 957.
[11] V.P. Malapure, S.K. Mitra, A. Bhattacharya, Numerical investigation of fluid flow and heat transfer over louvered fins in compact heat exchanger. Int. J. Thermal Sci. 46 (2007) 199.
[12] J.M. Ottino, S. Wiggins, Introduction: mixing in microfluidics. Phil. Trans. R. Soc. Lond. A 362 (2004) 923.
[13] H.A. Stone, A.D. Stroock, A. Ajdari, Engineering flows in small devices: microfluidics toward a lab-on-a-chip. Ann. Rev. Fluid Mech. 36 (2004) 381.
[14] S. Wiggins, J.M. Ottino, Foundations of chaotic mixing. Phil. Trans. R. Soc. Lond. A 362 (2004) 937.
[15] L. Lin, R. Ponnappan, J. Leland, High performance miniature heat pipe. Int. J. Heat Mass Transf 45 (2002) 3131.
[16] O. Aydin, M. Avci, Analysis of laminar heat transfer in micro-Poiseuille flow. Int. J. Thermal Sci. 46 (2007) 30.
[17] R.C. Chu, R.E. Simons, M.J. Ellsworth, R.R. Schmidt, V. Cozzolino, Review of cooling technologies for computer products. IEEE Trans. Device Materials Reliability 4 (2004) 568.
[18] I. Mudawar, Assessment of high-heat-flux thermal management schemes. IEEE Trans. Components Packag. Technol. 24 (2001) 122.
[19] F. Lefevre, M. Lallemand, Coupled thermal and hydrodynamic models of flat micro heat pipes for the cooling of multiple electronic components. Int. J. Heat Mass Transf 49 (2006) 1375.
[20] S.G. Kandlikar, High flux heat removal with microchannels – a roadmap of challenges and opportunities. Heat Transf Eng. 26 (2005) 5.
[21] S.S. Anandan, V. Ramalingam, Thermal management of electronics: a review of literature. Thermal Sci. 12 (2008) 26.
[22] S.V. Garimella, Advances in mesoscale thermal management technologies for microelectronics. Microelectronics J. 37 (2006) 1165.
[23] H. Peerhossaini, T. Lemenand, A thermal model for prediction of the Nusselt number in a pipe with chaotic flow. Appl. Thermal Eng. 22 (2002) 1717.
[24] D.R. Sawyers, M. Sen, H.-C. Chang, Heat transfer enhancement in three-dimensional corrugated channel flow. Int. J. Heat Mass Transf 41 (1998) 3559.
[25] A. Mokrani, C. Casterlain, H. Peerhossaini, The effects of chaotic advection on heat transfer. Int. J. Heat Mass Transf 40 (1997) 3089.
[26] N. Acharya, M. Sen, H.-C. Chang, Heat transfer enhancement in coiled tubes by chaotic mixing. Int. J. Heat Mass Transf 35 (1992) 2475.
[27] C. Chagny, C. Castelain, H. Peerhossaini, Chaotic heat transfer for heat exchanger design and comparison with a regular regime for a large range of Reynolds numbers. Appl. Thermal Eng. 20 (2000) 1615.
[28] S. Kimura, A. Bejan, The heatline visualization of convective heat transfer. ASME J. Heat Transf 105 (1983) 916.
[29] V.A.F. Costa, Bejan's heatlines and masslines for convection visualization and analysis. ASME Appl. Mech. Rev. 59 (2006) 126.
[30] S. Mahmud, R.A. Fraser, Visualizing energy flows through energy streamlines and pathlines. Int. J. Heat Mass Transf 50 (2007) 3990.
[31] A. Mukhopadhyay, X. Qin, S.K. Aggarwal, I.K. Puri, On extension of "heatline" and "massline" concepts to reacting flows through use of conserved scalars. ASME J. Heat Transf 124 (2002) 791.
[32] S. Banerjee, A. Mukhopadhyay, S. Sen, R. Ganguly, Natural convection in a bi-heater configuration of passive electronic cooling. Int. J. Thermal Sci. 47 (2008) 1516.
[33] F.-Y. Zhao, D. Liu, G.-F. Tang, Natural convection in a porous enclosure with a partial heating and salting element. Int. J. Thermal Sci. 47 (2008) 569.
[34] N.H. Saeid, Conjugate natural convection in a porous enclosure: effect of conduction in one of the vertical walls. Int. J. Thermal Sci. 46 (2007) 531.
[35] S.K. Aggarwal, A. Manhapra, Use of heatlines for unsteady buoyancy-driven flow in a cylindrical enclosure. ASME J. Heat Transf 111 (1989) 576.
[36] M.F.M. Speetjens, Topology of advective-diffusive scalar transport in laminar flows. Phys. Rev. E 77 (2008) 026309.
[37] H. Aref, Chaotic advection in perspective. Phys. Fluids 14 (2002) 1315.
[38] D. Beigie, A. Leonard, S. Wiggins, Invariant manifold template for chaotic advection. Chaos, Solitons & Fractals 4 (1994) 749.
[39] M.F.M. Speetjens, H.J.H. Clercx, G.J.F. van Heijst, Numerical and experimental study on chaotic advection in three-dimensional Stokes flows. J. Fluid Mech. 514 (2004) 77.
[40] M. Speetjens, G. Metcalfe, M. Rudman, Topological mixing study of non-Newtonian duct flows. Phys. Fluids 18 (2006) 103103.
[41] P.K. Kundu, Fluid Mechanics. Academic Press, London, 1990.
[42] J.M. Ottino, The Kinematics of Mixing: Stretching, Chaos and Transport. Cambridge University Press, Cambridge, 1989.
[43] J.M. Ottino, C.W. Leong, H. Rising, P.D. Swanson, Morphological structures produced by mixing in chaotic flows. Nature 333 (1988) 419.
[44] J.H.E. Cartwright, M. Feingold, O. Piro, Chaotic advection in three-dimensional unsteady incompressible laminar flow. J. Fluid Mech. 316 (1996) 259.
[45] K. Bajer, Hamiltonian formulation of the equations of streamlines in three-dimensional steady flows. Chaos, Solitons & Fractals 4 (1994) 895.
[46] E. Ott, Chaos in Dynamical Systems. Cambridge University Press, Cambridge, 2002.
[47] H.-C. Chang, M. Sen, Application of chaotic advection to heat transfer. Chaos, Solitons & Fractals 4 (1994) 955.
[48] M.S. Chong, A.E. Perry, B.J. Cantwell, A general classification of three-dimensional flow fields. Phys. Fluids A 2 (1990) 765.
[49] N. Malhotra, S. Wiggins, Geometric structures, lobe dynamics, and Lagrangian transport in flows with aperiodic time-dependence, with applications to Rossby wave flow. J. Nonlinear Sci. 8 (1998) 401.
[50] V.S. Malyuga, V.V. Meleshko, M.F.M. Speetjens, H.J.H. Clercx, G.J.F. van Heijst, Mixing in the Stokes flow in a cylindrical container. Proc. R. Soc. Lond. A 458 (2002) 1867.
[51] M.F.M. Speetjens, H.J.H. Clercx, G.J.F. van Heijst, Inertia-induced coherent structures in a time-periodic viscous flow. Phys. Fluids 18 (2006) 083603.
[52] M.F.M. Speetjens, H.J.H. Clercx, G.J.F. van Heijst, Merger of coherent structures in time-periodic viscous flows. Chaos 16 (2006) 043104.
[53] P. Mullowney, K. Julien, J.D. Meiss, Chaotic advection and the emergence of tori in the Küppers–Lortz state. Chaos 18 (2008) 033104.
[54] D.L. Vainchtein, A.I. Neishtadt, I. Mezic, On passage through resonances in volume-preserving systems. Chaos 16 (2006) 043123.
[55] C. Canuto, M.Y. Hussaini, A. Quarteroni, T.A. Zang, Spectral Methods in Fluid Dynamics. Springer, Berlin, 1987.
[56] P.D. Anderson, O.S. Galaktionov, G.W.M. Peters, F.N. van de Vosse, H.E. H. Meijer, Analysis of mixing in three-dimensional time-periodic cavity flows. J. Fluid Mech. 386 (1999) 149.